International Journal of Thermophysics, Vol. 25, No. 2, March 2004 (© 2004)

Thermal Diffusivity Measurement of Isotopically Enriched 28-Si Single Crystal by Dynamic Grating Radiometry[1]

Y. Taguchi[2, 3] and Y. Nagasaka[2]

In the past decade it has been suggested that the isotopic enrichment of 28-silicon enhances its thermal properties. Thus, 28-silicon is suitable as a heat sink in large-scale integrated circuits. Although some studies have focused on the measurement of isotopically enriched silicon's thermal properties, accurate experimental data are not sufficient because of this material's high conductivity and large heat capacity which make measurement difficult. However, the dynamic grating radiometry (DGR) method has been successfully developed to measure the thermal diffusivity of 28-silicon. In the DGR method, the sample is heated by interference of two pulsed laser beams, and the temperature decay is monitored by an infrared detector. By analyzing the temperature changes of the peaks and valleys of the thermal grating, the thermal diffusivities parallel and perpendicular to the sample surface are obtained simultaneously. In this paper, the optimum conditions of the experimental setup for measuring isotopically enriched silicon are discussed. The comparison of thermal diffusivities between 28-silicon and natural silicon (with a thickness of about 100 μm) is presented, and the applicability of DGR to isotope engineering is reported.

KEY WORDS: dynamic grating radiometry; high-conductivity thin film; isotope engineering; isotopically enriched 28-silicon; thermal diffusivity.

1. INTRODUCTION

In recent years, the thermal properties of electronic devices have become increasingly important in the thermal design of large-scale integrated

[1] Paper presented at the Fifteenth Symposium on Thermophysical Properties, June 22–27, 2003, Boulder, Colorado, U.S.A.

[2] Department of System Design Engineering, Keio University, 3-14-1 Hiyoshi, Yokohama 223-8522, Japan.

[3] To whom correspondence should be addressed. E-mail: tag@naga.sd.keio.ac.jp

0195-928X/04/0300-0459/0 © 2004 Plenum Publishing Corporation

circuits in which the density of heat sources increases exponentially ($\sim 100\ \mathrm{W \cdot cm^{-2}}$). However, it is very difficult to measure the thermal properties of micro-scale device configurations (i.e., heat sinks and semiconductors) because of the high conductivity and anisotropy that is caused by their production processes. Therefore, we have developed the dynamic grating radiometry (DGR) method to measure the anisotropic thermal diffusivity of high-conductivity films *in situ* in electronic circuits. We have also described the applicability of DGR for measurements on orthotropic graphite sheets and highly oriented diamond films [1, 2].

In isotope engineering [3], it is theoretically expected that the thermal properties of isotopically enriched 28-silicon (28-silicon: 99.924 at%) are superior to those of natural silicon. Isotopically enriched silicon can be applied as a substrate of ultra large-scale integration (ULSI) for heat dissipation purposes. The mechanisms of phonon scattering in silicon are as follows: (1) scattering by the isotope (29-silicon and 30-silicon); (2) scattering by the sample boundary; (3) pointing defects or lattice imperfections; (4) obeying the normal process; and (5) obeying the Umklapp process. Thus, in isotopically pure 28-silicon, the effect of isotopic composition (descending the phonon scattering by the isotope) may affect the enhancement of its thermal properties. However, only few accurate data have been reported concerning the significant difference of thermal properties between 28-silicon and natural silicon because of its small light absorption coefficient, large heat capacity, and its high conductivity which make it difficult to measure. Moreover, there has been no contact-free technique to measure the thermal properties of semiconductors and insulators, which can be applied for in-process control. Hence, a technique for the *in situ* measurement of thermal properties is required to satisfy these demands.

In the present paper, the optimum experimental setups of DGR for measuring 28-silicon are reported. By using the focused Gaussian laser beam in the heating process, the heat loss toward the outside of the heating area and the influence of oxidization are significant. In addition, the effect of the noise factor, which impacts the dispersion and deviation of the experimental results, is described. Finally, we will discuss the difference in results between 28-silicon and natural silicon for the experiments using DGR. The applicability of DGR to isotope engineering is also studied.

2. MEASUREMENT THEORY

In the DGR method, the sample is heated by the interference fringe pattern of two laser beams. The temperature change due to the two-dimensional heat conduction parallel and perpendicular to the sample is monitored as a change of an infrared signal (Fig. 1). In order to consider

the two-dimensional heat conduction, we assume that the sample surface is uniformly and instantaneously heated by the laser grating, and the boundaries of the semi-infinite sample surface are adiabatic. In this case, the solution of the two-dimensional heat conduction equation is described as

$$T_{xz}(x, 0, t) = \left\{ T_0 + T_1 \exp\left(-\frac{t}{\tau_x}\right) \cos\left(\frac{2\pi x}{\Lambda}\right) \right\} \times \left\{ \exp\left(\frac{t}{\tau_z}\right) \operatorname{erfc}\left(\sqrt{\frac{t}{\tau_z}}\right) + \Delta T_f(0, t) \right\}, \quad (1)$$

$$\tau_x = \frac{1}{a_x}\left(\frac{\Lambda}{2\pi}\right)^2 \quad \text{and} \quad \tau_z = \frac{1}{a_z \alpha^2},$$

where T_0 is the mean initial temperature rise, T_1 is the spatial temperature distribution, Λ is the fringe space, and τ is the time constant of each direction, which are defined with the thermal diffusivities $a_{x,z}$ and light absorption coefficient α [1]. The $\Delta T_f(0, t)$ is the temperature rise that occurs due to the effect of sample thickness [2].

However, it is impossible to determine both time constants in Eq. (1), because the equation is the product of two simple decays. By utilizing the pattern of sinusoidal temperature distribution, which is monitored by the

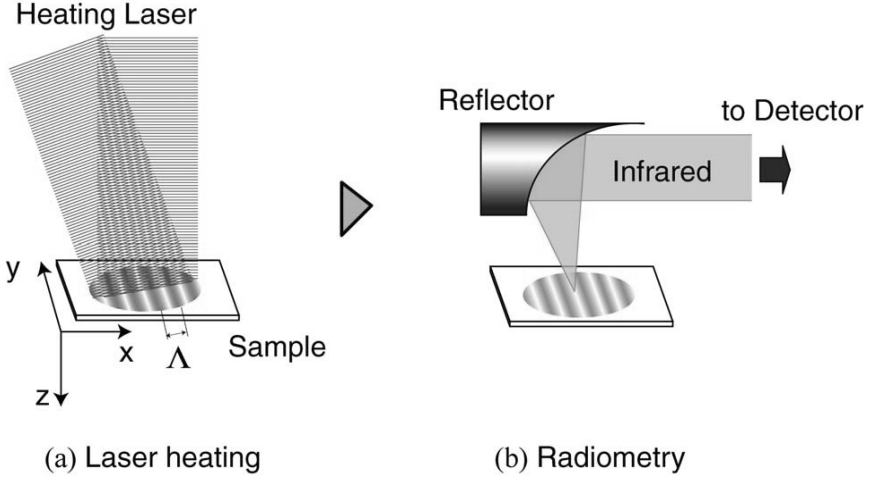

Fig. 1. Principle of dynamic grating radiometry (DGR). (a) The sample is heated by the interference fringe pattern of two pulsed laser beams. The fringe space Λ is around 200 to 500 μm. (b) The temperature distribution of the sample is monitored via infrared thermometry as a function of two-dimensional heat conduction.

scanning system of two laser beams, we are able to separate the thermal diffusivities parallel and perpendicular to the plane in Eq. (1). When the reflectors condense the emission from both extremes of the peaks and valleys of the sinusoidal temperature distribution, the exact shapes of the temperature changes are expressed as

$$T_P = T_{xz}(0, 0, t), \qquad T_V = T_{xz}(\Lambda/2, 0, t), \tag{2}$$

where T_P and T_V are the temperature decays of a peak and valley, respectively. Then, the heat conduction in the z- and x-directions are separated by using a peak and valley (Eqs. (2)) of thermal grating as follows:

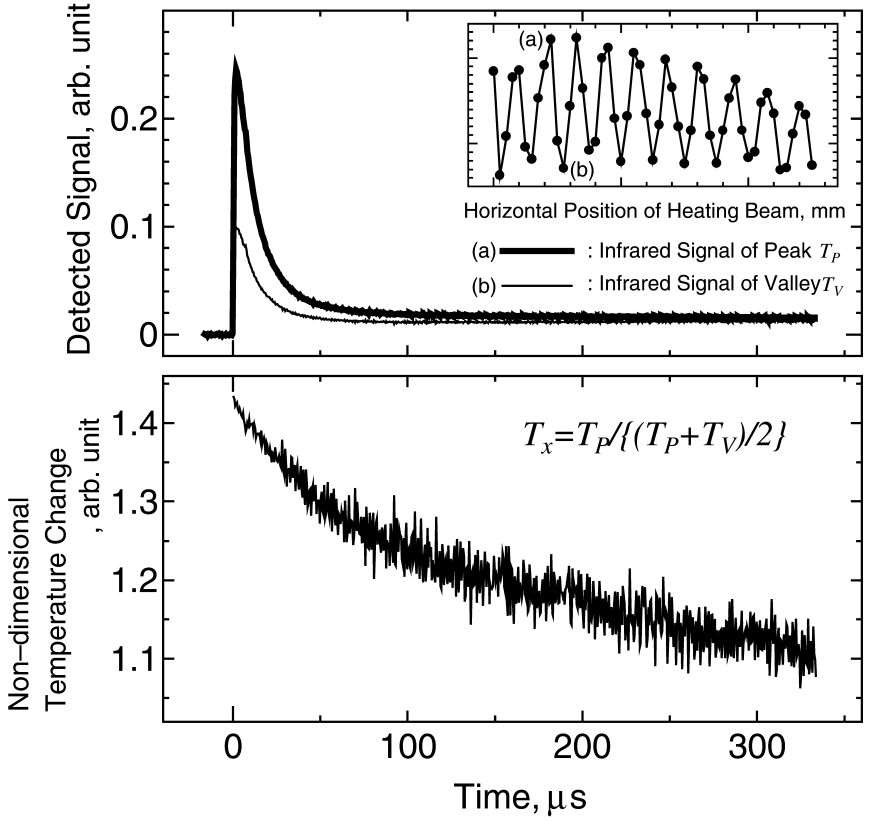

Fig. 2. Typical example of temperature change. Upper diagram: The inset shows the thermal grating detected by scanning thermometry. (a) is defined as a peak and (b) as a valley of the interference pattern. Lower diagram: Non-dimensional temperature change includes the information regarding heat conduction parallel to the sample surface.

$$T_z = \frac{1}{2}\{T_P(0, 0, t) + T_V(\Lambda/2, 0, t)\}$$

$$= T_0 \left\{ \exp\left(\frac{t}{\tau_z}\right) \operatorname{erfc}\left(\sqrt{\frac{t}{\tau_z}}\right) + \Delta T_f(0, t) \right\}, \quad (3)$$

$$T_x = \frac{T_P}{(T_P + T_V)/2} = 1 + \frac{T_1}{T_0} \exp\left(-\frac{t}{\tau_x}\right). \quad (4)$$

By using the decay signals of the temperature distribution of the two extremes (the peak and valley), the non-dimensional temperature change that includes information on the horizontal thermal diffusivity is determined by Eq. (4). Figure 2 illustrates (a) the typical temperature distribution of the results of scanning and the temperature changes at the extreme of thermal grating, and (b) the non-dimensional temperature change analyzed by Eq. (4). Hence, with DGR, we can extract the thermal diffusivities parallel and perpendicular to the plane separately.

3. EXPERIMENTAL APPARATUS

A schematic image of the present experimental apparatus is illustrated in Fig. 3. To create the transient thermal gradient instantaneously, a Nd:YAG Q-switched pulse laser (NEW WAVE Res.: power 50 mJ · 5 ns^{-1} at 532 nm wavelength with a repetition rate up to 10 Hz) is adopted. A beam expander, which has a diopteral controller, is employed to generate a high-contrast sinusoidal temperature distribution on the sample surface which is composed of a material having a large heat capacity and small absorption coefficient, such as silicon. A pulsed high-power laser beam is divided by a beam splitter into two beams of equal intensity. Two beams are intersected on the sample surface by mirrors under an angle θ (θ is determined from the distance between M3 and M5) and generate an optical interference fringe pattern whose intensity distribution is spatially sinusoidal. In order to monitor the decay of the temperature distribution caused by the heat conduction process, we employ infrared thermometry by measuring the thermal radiation emitted from a spot on the sample surface. The nano-order moving system, which shifts the position of the heated area on the sample, is used to scan the sample surface and to observe the exact shape of the interference fringe pattern. Off-axis paraboloidal mirrors (the spatial resolving diameter δ is estimated to be 80 to 100 μm) condense the emission from a sample to the LN_2-cooled HgCdTe infrared detector (Fermionics: PVA-500-20), and the weak signal is amplified by a current-voltage preamplifier (bandwidth of 20 MHz) and voltage-voltage amplifier

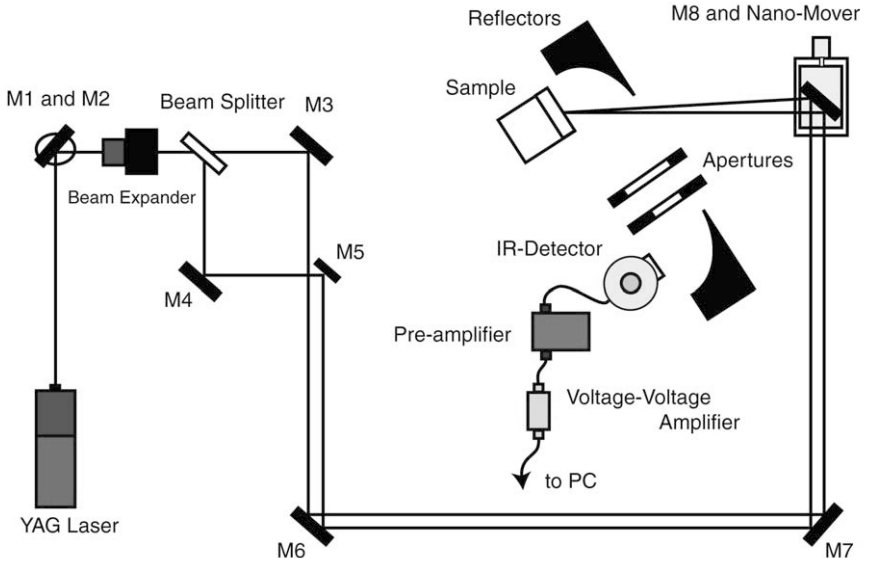

Fig. 3. Experimental apparatus of DGR.

(cutoff frequency of 200 MHz). The detected signal is averaged for a hundred laser pulses in order to significantly improve the S/N ratio.

4. OPTIMUM CONDITIONS FOR MEASURING SILICON

4.1. Effect of the Gaussian Distribution of the Heating Laser

For the purpose of measuring the thermal diffusivity parallel to the plane, it is postulated in the idealized theoretical condition that the sample be heated uniformly by a pulsed-laser beam, and the effect of the non-uniform laser heating caused by the Gaussian laser distribution has not been considered. However, in the case of local area heating using a TEM_{00} laser beam, especially $\Lambda \sim w/2$ (w: Gaussian radius of heating laser), the influence of heat loss toward the outside of the heating area is not insignificant.

In order to solve the heat conduction equation, which is considered the effect of the Gaussian radius of the heating laser, Green's function at (x, y, z) at the time t is adopted [4]. Green's function is most conveniently defined for the closed surface as the potential that vanishes over the surface. The assumptions of two-dimensional heat conduction parallel to the plane are as follows: (1) the sample is a semi-infinite solid ($-\infty < x < \infty$, $0 < z < \infty$), (2) there is no inner heat source in the sample,

and (3) the sample surface boundaries are adiabatic. In this case of two-dimensional heat conduction, Green's functions in a sample are given by

$$G_{Gx}(x, t\,;\, x', t') = \frac{1}{2\sqrt{\pi a_x\,(t-t')}}\left[\exp\left\{\frac{-(x-x')^2}{4a_x\,(t-t')}\right\}\right], \tag{5}$$

$$G_{Gz}(z, t\,;\, z', t') = \frac{1}{2\sqrt{\pi a_z\,(t-t')}}\left[\exp\left\{\frac{-(z+z')^2}{4a_z\,(t-t')}\right\}+\exp\left\{\frac{-(z-z')^2}{4a_z\,(t-t')}\right\}\right]. \tag{6}$$

The initial temperature distribution on the x-axis $\Psi_{Gx}(x)$ and z-axis $\Psi_{Gz}(z)$ are given by the following equations:

$$\Psi_{Gx}(x) = \left\{1+Vi\cos\left(\frac{2\pi x}{\Lambda}\right)\right\}\exp\left(-\frac{2x^2}{w^2}\right), \tag{7}$$

$$\Psi_{Gz}(z) = \exp(-\alpha z), \tag{8}$$

where Vi is the visibility of an interference fringe pattern. The exact profile of the temperature distribution on the sample surface is described as

$$\begin{aligned} T_G(x, 0, t) &= \int G_{Gx}(x, t\,;\, x', 0)\,\Psi_{Gx}(x')\,dx' \int G_{Gz}(z, t\,;\, z', 0)\,\Psi_{Gz}(z')\,dz' \\ &= \Gamma\left\{1+Vi\exp\left(-\frac{W}{\tau_x}t\right)\cos\left(\frac{2\pi}{\Lambda}W x\right)\right\} \\ &\quad\times\left\{\exp\left(\frac{t}{\tau_z}\right)\mathrm{erfc}\left(\sqrt{\frac{t}{\tau_z}}\right)+\Delta T_{\mathrm{f}}(0, t)\right\}, \end{aligned} \tag{9}$$

where

$$\Gamma = \frac{w}{\sqrt{8a_x\,t+w^2}}\exp\left(-\frac{2x^2}{8a_x\,t+w^2}\right) \quad \text{and} \quad W = \frac{w^2}{8a_x\,t+w^2}. \tag{10}$$

According to Eq. (9), the time constant τ_x and the fringe space Λ are expanded by W, and the span of detection time may directly affect the results of the curve fitting analysis. In using the procedure to separate the thermal diffusivities parallel and perpendicular to the plane (see Section 2), it will be complicated to estimate the error that occurs from heat leaking into the unheated region. In order to evaluate the thermal diffusivity error due to the Gaussian intensity distribution of the heating laser, numerical data of non-dimensional temperature change, which is calculated by Eq. (9), is fitted by the ideal Eq. (4). Comparing the theoretical value and

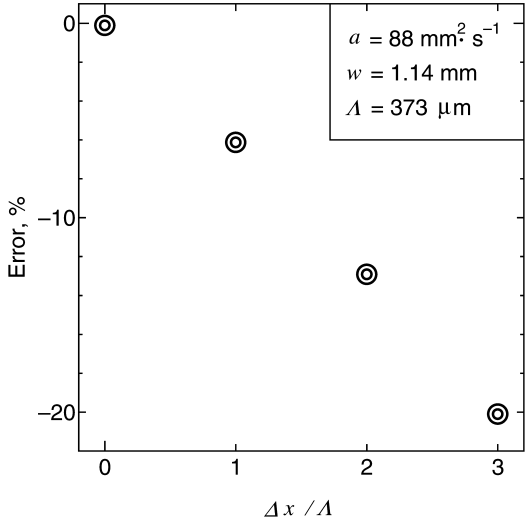

Fig. 4. Effect of the Gaussian intensity distribution of the heating laser beam as a function of $\Delta x/\Lambda$ at $\Lambda = 373$ μm for a typical example of Gaussian radius $w = 1.14$ mm. Δx is the distance from the center of the laser beam, and the error is calculated as the thermal diffusivity. Error $= (a_{\text{fit}} - a_{\text{theory}})/a_{\text{theory}} \times 100$.

the results of curve fitting, the interrelationship between the effect of heat loss toward the outside of the heating area and the position of the detected signals is confirmed. In Fig. 4, the error of the thermal diffusivity is inversely proportional to the distance from the center of the heated area $\Delta x/\Lambda$. Thus, by analyzing the signals of the peak and valley that are close to the center of the beam, we can eliminate the influence of non-uniform Gaussian heating.

4.2. Effect of Signal/Noise Factor

In fitting the signal that has normal-mode noise, white noise may have practically no influence in the results. In the DGR method, for the purpose of reducing the background noise (e.g., background radiation, the pointing stability of the heating laser, and electronic noise), the infrared signal is electrically averaged for a hundred laser pulses (e.g., up to 40 dB at a low signal of silicon) by means of a digital storage oscilloscope. However, in the procedure to separate the thermal diffusivity parallel and perpendicular to the sample (see Eq. (4)), the influence of its noise is conspicuous. Moreover, it is predicted that the results of analysis may have dispersion or a

deviation of the time constant and thermal diffusivity. In this section, the effect of the noise factor is considered, and the optimum condition of the averaging number of laser pulses is reported.

In order to estimate the dispersion or deviation of the thermal diffusivity, the numerical model of the temperature distribution including the normal-mode noise (based on Eq. (9)) is considered. The numerical data (the peak and valley signals close to the center of the heating area) are analyzed as a non-dimensional temperature change by Eq. (4). Figure 5 illustrates the numerical simulation of natural silicon based on Eq. (9) for various signal/noise ratios (S/N ratio). In the case of a low S/N ratio (i.e., 30 dB, 100 averaging points), the analyzed thermal diffusivities are very widely dispersed. In addition, under these circumstances, the mean thermal diffusivity is 12% smaller than the theoretical value. On the other hand, at a high S/N ratio (i.e. 40 dB, 1000 averaging points), the dispersion of results are within 5%, and the deviation of the mean value of the thermal diffusivity is within about −2%. As mentioned above, whereas the deviation of the mean thermal diffusivity is improved by increasing the S/N ratio, the reproducibility of fitting results is not dramatically improved. In the present work, the number of averaging points is set to ∼ 1000 to reduce the influence of the noise factor.

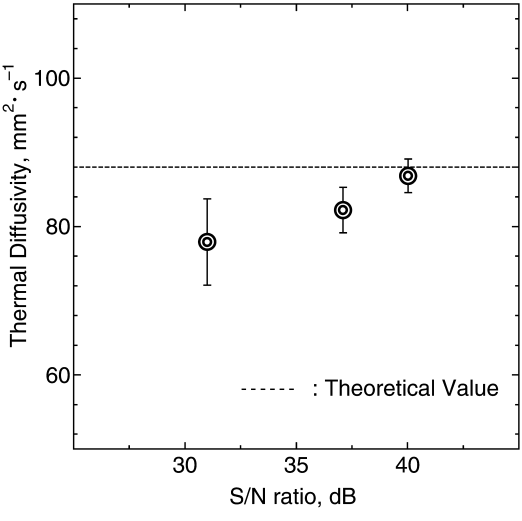

Fig. 5. Influence of noise factor. The numerical data that includes the normal-mode noise are analyzed by Eq. (4). The mean value of the thermal diffusivity parallel to the plane and standard deviation of the mean are demonstrated.

5. RESULTS AND DISCUSSIONS

Natural silicon is composed of three different isotopes: 28-silicon (92.2 at%), 29-silicon (4.7 at%), and 30-silicon (3.1 at%). Takyu et al. [6] have successfully grown an isotopically enriched 28-silicon by using the gas centrifuge technique to separate 28-silicon stable isotopes, and the floating-zone method (FZ) for the subsequent growth of an isotopically enriched bulk 28-silicon crystal. In this section, the applicability of DGR to measure the thermal diffusivity of isotopically enriched 28-silicon is discussed. For the experimental investigation of the possible enhancement of the thermal properties by isotopic enrichment, specimens of 28-silicon and natural silicon (whose specifications are listed in Table I) are demonstrated at room temperature.

In order to produce a high-contrast thermal image of the interference fringe pattern and achieve a high visibility of the detected signal, a new optical system (i.e., laser focusing lenses and two apertures) and a new monitoring system (i.e., a voltage-voltage amplifier and electrical averaging component) are utilized. A typical scanning image of silicon under the new experimental setup is illustrated in Fig. 6, showing a drastic improvement in the modulation transfer function (MTF). Comparing the image of the thermal grating with that of the optical image of a CCD camera, the spatial resolving power is estimated to be about 80 μm.

The experimental results for 28-silicon and natural silicon are summarized in Table II. Figure 7 compares the data regarding the thermal diffusivity of natural silicon and 28-silicon. The signals of a peak and a valley are located at the center of the laser beam in order to mitigate the effect of the Gaussian temperature distribution with modeling described in Section 4.1. First of all, attending to the results of natural silicon, the data spread of thermal diffusivity (experimental standard deviation of the mean; experimental SDOM) is within $\pm 6\%$, and the repeatability of DGR is confirmed. As mentioned in Section 4.2, for the condition of $S/N = 38$ dB, the experimental SDOM is theoretically calculated as $\pm 4\%$; thus, the experimental results are in agreement with the predictions obtained by

Table I. Specifications of Isotopically Enriched 28-Silicon

		Isotope composition [6]		
	Thickness (μm)	28-silicon	29-silicon	30-silicon
natural silicon	(nominal) 130	92.2 at%	4.7 at%	3.1 at%
28-silicon	(nominal) 120	99.93 at%	0.07 at%	0 at%

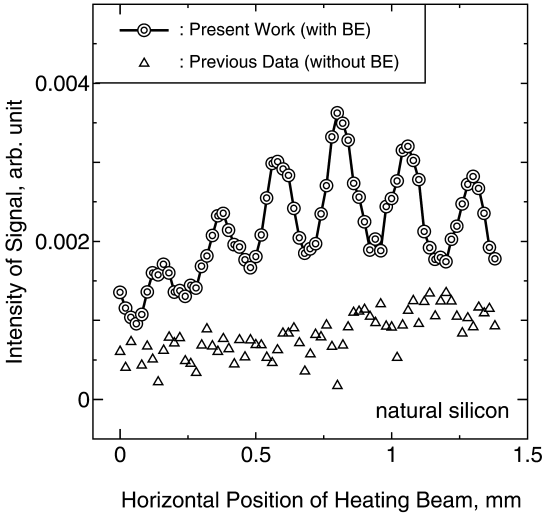

Fig. 6. Improvement of contrast in the case using the condensing lens in order to increase the density of the heating energy. The visibility of the thermal grating is clearly increasing compared to the case without the condensing lens. The optical image is observed by a CCD camera at the same time. $Vi = 0.62$ and $\Lambda = 205$ μm.

numerical simulation. The uncertainty of the present work for measuring natural silicon is estimated to be about $\pm 9\%$ (based on GUM). Under such noisy conditions, according to Fig. 5, it was assumed that the mean value of the thermal diffusivity would be 7% smaller than that of the recommended value. However, the deviation of the experimental results was slightly larger than its predicted value. Due to the high power laser beam adsorption (i.e., silicon dioxide and carbon adsorber) and the emissive heat loss (silicon is transparent in the near-infrared region), the thermal diffusivity may have a tendency to be inferior to that of the predicted value. In DGR, considering the ideal condition of uniform laser heating, the emissive heat loss ΔT_{ems} in the z-direction is expressed as

$$T_{xz}(x, 0, t) = \left\{ T_0 + T_1 \exp\left(-\frac{t}{\tau_x}\right) \cos\left(\frac{2\pi x}{\Lambda}\right) \right\} \times \left\{ \exp\left(\frac{t}{\tau_z}\right) \operatorname{erfc}\left(\sqrt{\frac{t}{\tau_z}}\right) + \Delta T_{\text{f}}(0, t) - \Delta T_{\text{ems}} \right\}. \quad (11)$$

Table II. Experimental Results Regarding Natural Silicon and 28-Silicon

		Thermal diffusivity ($mm^2 \cdot s^{-1}$)		Reproducibility[e]
Present work	natural silicon	65.5	: a_x	±6%
	28-silicon[a]	116	: a_x	±8%
TPRC [5]	natural silicon	88	: a_z	N/A
Ruf et al. [7]	28-silicon[b]	143	: a_z	N/A
Gusev et al. [10]	28-silicon[c]	95.3	: a_z	N/A
Itoh et al. [11]	28-silicon[d]	111	: a_z	N/A

[a] Composition of isotope silicon; 28-silicon (99.93 at%), 29-silicon (0.07 at%), 30-silicon (0 at%).

[b] Composition of isotope silicon; 28-silicon (99.859 at%), 29-silicon (0.127 at%), 30-silicon (< 0.2 at%).

[c] Composition of isotope silicon; 28-silicon (99.896 at%), 29-silicon (0.09 at%), 30-silicon (0.014 at%).

[d] Composition of isotope silicon; 28-silicon (99.9 at%).

[e] Experimental standard deviation of the mean.

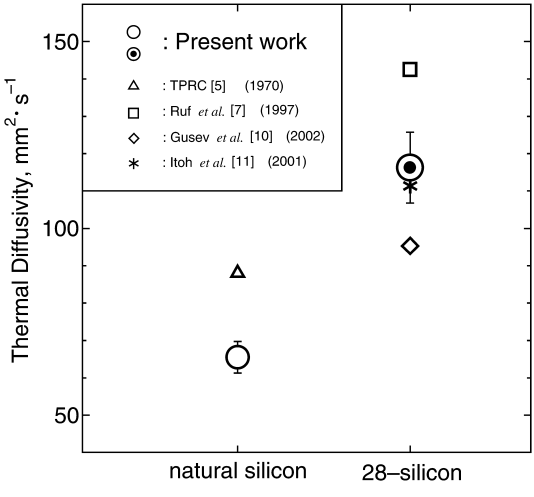

Fig. 7. Comparison of the experimental results regarding natural silicon and 28-silicon. The fringe space $\Lambda = 373$ μm and the Gaussian radius $w = 1.14$ mm. The results are dispersed by the noise factor (see Section 4.2). Other experimental results and the results of simulation are also shown.

Thus, by using the procedure to separate the thermal diffusivity parallel and perpendicular to the sample (Eq. (4)), the heat loss ΔT_{ems} is negligible in a non-dimensional temperature change. Moreover, it is possible to reduce the effect of oxidization and adsorption by controlling the energy of the heating laser beam. In the case of 28-silicon, the S/N ratio of signal is estimated to be 25 dB; thus, the dispersion of experimental results is calculated as $\pm 6\%$ by numerical estimation (see Section 4.2). The reproducibility of this experimental result agrees with the numerical estimation. Ruf et al. [7] have measured the 28-silicon (composition of isotope silicon: 28-silicon (99.859 at%), 29-silicon (0.127 at%), and 30-silicon (< 0.2 at%)) using a steady-state heat-flow method, and they have indicated a 60% enlargement of thermal conductivity by isotopic enrichment. In addition, by using a transient pump-probe method (Capinski et al. [8]), a 60% enhancement of thermal conductivity at 300 K has been observed. However, Inyushkin et al. [9] have suggested that isotopic enrichment will not dramatically affect the improvement of thermal properties. Also, Gusev et al. [10] have revealed a 7% difference of thermal conductivity between natural silicon and 28-silicon based on experimental results by using a steady-state method. In an earlier numerical simulation of isotopically enriched silicon (Itoh et al. [11]), the increase in thermal conductivity of 28-silicon has been estimated to be 25% at room temperature. In the present work, assuming that the measurements of natural silicon and 28-silicon have the same systematic error of laser beam adsorption, the thermal diffusivity parallel to the sample surface of 28-silicon was 77% larger than that of natural silicon. Although there is ample scope to discuss the absolute value of the thermal properties of 28-silicon, we can confirm the applicability of DGR to measure isotopically enriched 28-silicon within a 9% uncertainty and the validity of our method for application to isotope engineering.

ACKNOWLEDGMENTS

The authors would like to acknowledge Prof. K. M. Itoh of Keio University for supplying 28-silicon and for his exciting discussions. The work described in this paper was financially supported in part by the Science and Technology Agency of Japan under the Promotion System for Intellectual Infrastructure of Research and Development.

REFERENCES

1. Y. Taguchi and Y. Nagasaka, *Int. J. Thermophys.* **22**:1 (2001).
2. Y. Taguchi and Y. Nagasaka, *Trans. Jpn. Soc. Mech. Eng. B* **68**:665 (2002). (in Japanese)

3. M. Asen-Palmer, K. Bartkowski, E. Gmelin, M. Cardona, A. P. Zhernov, A. V. Inyushkin, A. Taldenkov, V. I. Ozhogin, K. M. Itoh, and E. E. Haller, *Phys. Rev. B* **56** (1997).
4. H. S. Carslaw and J. C. Jaeger, *Conduction of Heat in Solids*, 2nd edn. (Oxford University Press, London, 1959), pp. 449–460.
5. Y. S. Touloukian, R. W. Powell, C. Y. Ho, and P. G. Kemens, *Thermal Conductivity—Metallic Elements and Alloys TPRC Data* (IFI/Plenum Press, New York/Washington, 1970), p. 339.
6. K. Takyu, K. M. Itoh, K. Oka, N. Saito, and V. I. Ozhogin, *Jpn. J. Appl. Phys.* **38**:12B (1999).
7. T. Ruf, R. W. Henn, M. Asen-Palmer, E. Gmelin, M. Cardona, H.-J. Phol, G. G. Devyatych, and P. G. Sennikov, *Solid State Commun.* **115** (2000).
8. W. S. Capinski, H. J. Maris, E. Bauser, I. Silier, M. Asen-Palmer, T. Ruf, M. Cardona, and E. Gmelin, *Appl. Phys. Lett.* **71**:15 (1997).
9. A. V. Inyushkin, *Inorg. Mater.* **38**:5 (2002).
10. A. V. Gusev, A. M. Gibin, O. N. Morozkin, V. A. Gavva, and A. V. Mitin, *Inorg. Mater.* **38**:11 (2002).
11. K. M. Itoh and K. Takyu, *Jpn. J. Appl. Phys.* **70**:10 (2001). (in Japanese)